JOURNAL OF GEOPHYSICAL RESEARCH, VOL. 97, NO. C6, PAGES 9507-9520, JUNE 15, 1992

THE RESPONSE OF THE SOUTH BRAZIL BIGHT TO THE PASSAGE OF WINTERTIME COLD FRONTS

José L. Stech and João A. Lorenzzetti

Divisão de Ciências da Terra, Instituto Nacional de Pesquisas Espaciais, Secretaria Especial de Ciência e Tecnologia da Presidência da República, São José dos Campos, Brazil

Abstract. On the southeastern continental shelf of Brazil the wintertime subtidal variability of the circulation is highly dominated by the passage of cold fronts. Hydrographic data for the region reveal that during this (July, August, September) season only a weak vertical stratification is observed. In this paper the response of the region to cold fronts is studied by using a barotropic finite element model, forced by a conceptual cold front wind field derived from the analysis of coastal winds and satellite imagery.

1. Introduction

The South Brazil Bight (SBB) is defined as the region of the southeastern Brazilian continental shelf extending from Cabó São Tomé (22°00'S and 41°00'W) to Cabo Santa Marta (28°00'S and 48° 49'W) [Castro Filho, 1985]. The shelf width varies from 70 km at Cabo Frio to a maximum of 200 km at Santos midsection. The bottom topography is relatively smooth, with the isobaths tending to follow the coastline. The shelf break is located between the 150- and 200-m isobaths (Figure 1).

Hydrographic data collected in the SBB by several investigators show a strong thermocline and pycnocline present at a depth of 25 to 30 m during the summer season. During the winter season, the mixed layer is generally well developed over most of the shelf, with the water column showing only small temperature and density variations over its depth [Miranda, 1982; Matsuura, 1983; Castro Filho, 1985; Castro Filho et al., 1987]. Figure 2 from Miranda [1982] shows very clearly, for two nearby vertical cross-shelf sections close to São Sebastião, this strong difference in stratification between summer and winter for the SBB.

According to Clarke and Brink [1985], the shelf response to low-frequency forcing is dominated by its barotropic mode when the following condition is satisfied: $N^2 f^{-2} s^2 << 1$, where N is the shelf average Brunt-Vaisalla frequency, f is the Coriolis parameter and s is the average shelf bottom slope. Ikeda and Stevenson [1982] and Leite [1983] show that typical values of N for the winter season in the SBB are in the range of 1.5×10^{-3} to 8.3×10^{-3} Hz. The bottom slope parameter varies between 0.5×10^{-3} to 1.0×10^{-3}. The Coriolis parameter is here taken as 0.6×10^{-4} s^{-1}, corresponding to the midsection latitude of 25°S. Therefore $N^2 f^{-2} s^2$ varies between 1.6×10^{-4} and 1.9×10^{-2}, implying a high barotropic response of the SBB. The baroclinic component of the flow is expected to become enhanced in the region of the shelf break, where intrusions of the Brazil Current can affect the flow [Garfield, 1990].

At subtidal frequencies and especially during the winter, the surface wind field in the SBB is highly influenced by the passage of frontal systems occurring over periods of 6 to 11 days [Stech, 1990]. Considering that the wind stress is one of the major low-frequency forcing mechanisms of the coastal circulation, the frontal systems are expected to play a significant role in determining variability in the flow.

Several studies have been done dealing with the response of the continental shelf to the wind stress field associated with weather systems traveling across the coastline. For example, Chao [1981] studied the barotropically forced circulation over the continental shelf, generated by an alongshore wind stress having a finite extent in the alongshore direction and oscillating with a frequency typical of the frontal passages. His work treated the interaction of barotropic shelf waves with the localized wind-forced response.

Paper number 92JC00486.
0148-0227/92/92JC-00486$05.00

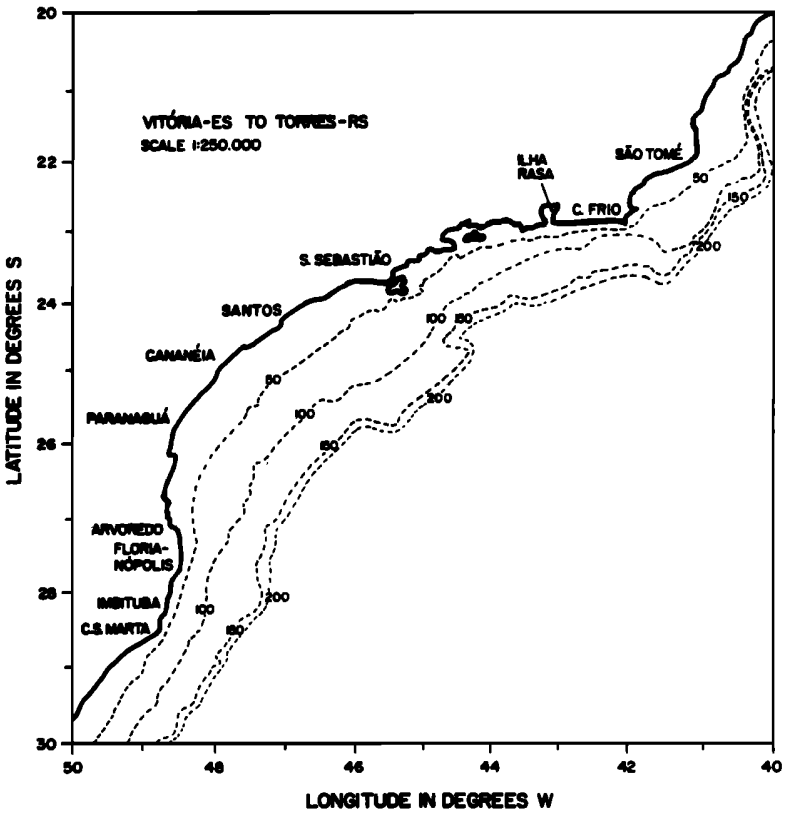

Fig. 1. Map of the meteorological station station positions and the South Brazil Bight (SBB) with isobaths (dashed lines) in meters.

Klinck et al. [1981] investigated the circulation induced over the continental shelf by a moving, localized line of surface stress. In that paper the shelf response is analyzed in terms of the ratio of the storm speed to the internal or external wave speed depending on the degree of baroclinicity of the flow.

In the present paper the wintertime response of the SBB to the passage of frontal systems is investigated through a wind forced barotropic numerical model that incorporates all terms of the Navier-Stokes equations, real bottom topography and coastline geometry. The model is forced by a wind stress field which simulates the main characteristics of the real wind field associated with the passage of cold fronts in the southeast Brazilian coast.

2. Data Set and Processing

Surface wind data collected at 0, 6, 12 and 18 hours (local time) were available for the winter season from the coastal stations of Santa Marta, Arvoredo, Ilha Rasa and São Tomé (see Figure 1 for stations locations) for the years 1980 to 1985. In order to get a clearer signal of the low-frequency synoptic band associated with the weather systems, a low-pass Lanczos square filter with a cutoff period of 40 hours was applied to the data set.

The energy spectra of the (6 hour intervals) wind series collected in the winter of 1984 at the Santa Marta station (90 days) are presented in Figure 3, for both the alongshore and cross-shore components. The spectra were calculated through the Fourier transform of the auto-covariance function. It can be observed that most of the energy is located in the alongshore component. Two main energy peaks dominate the spectrum; one at 11 days and the other at 6.5 days. For the São Tomé station (not shown) the 6.5 day peak was found to dominate the spectrum. The following analysis of satellite imagery shows that the 6.5-day period is associated with the passage of cold fronts. Wind energy spectra for the other years, not shown, have the same characteristics.

In order to get a better picture of how the frontal systems propagate through the region and to fill in gaps in the data set, visible and infrared images of the GOES-W satellite, as well as surface synoptic charts were analyzed for the same 6-year period. Figure 4 shows an example of a time sequence of cold front penetration as

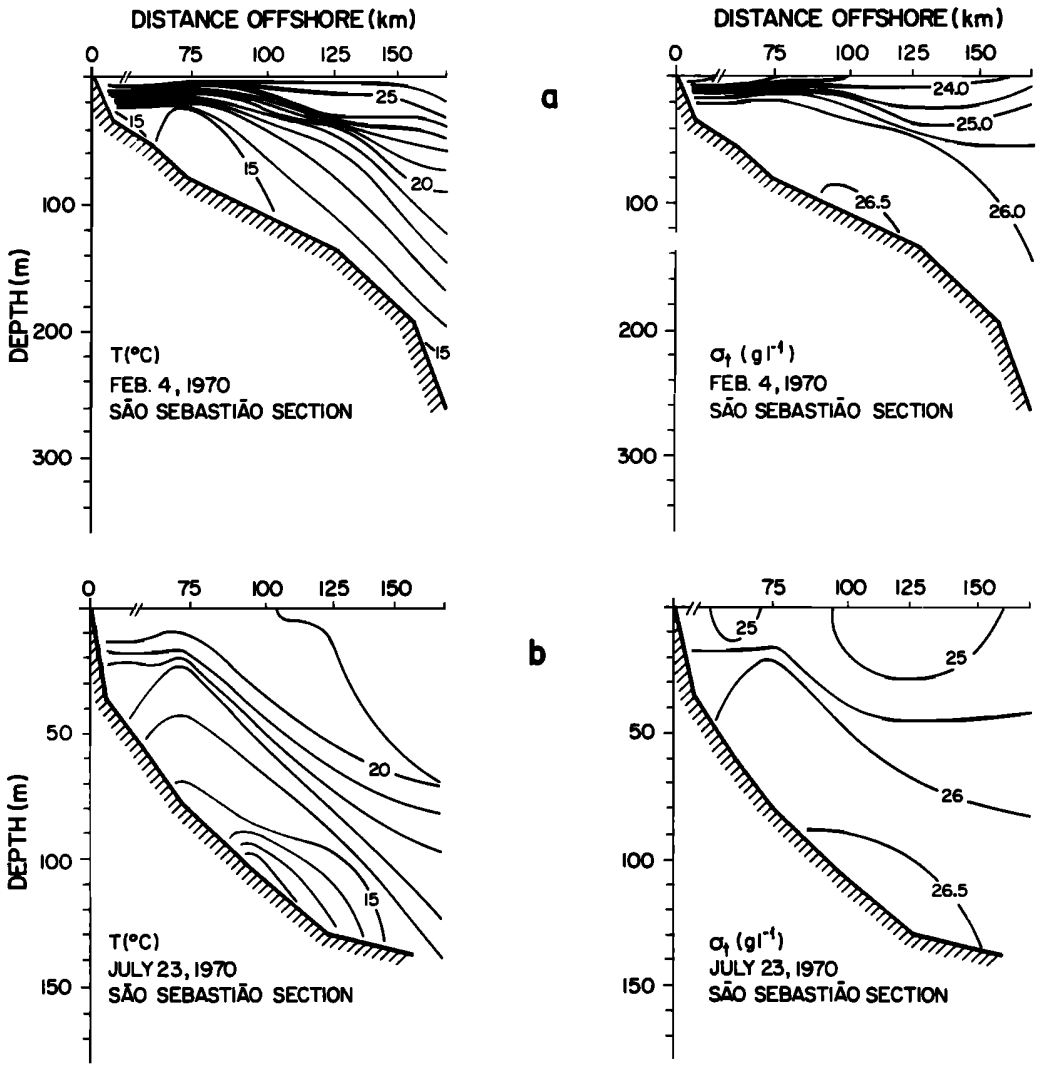

Fig. 2. Vertical distribution of the temperature (degrees Celsius) and sigma-t (gram per liter) along two cross-shelf sections near São Sebastião for the (a) summer and (b) winter of 1970. From Miranda [1982].

observed by the IR sensor of the GOES satellite, and Figure 5 shows the two surface synoptic charts for the same period. Table 1 presents some results of this analysis. As can be seen from Table 1, the 6.5-day peak present in the spectra of the wind matches with the mean time between consecutive fronts, supporting the proposition that this peak is associated with the passage of frontal systems.

Sea level data (sampled at hourly intervals) collected at several coastal tide gauge sites were also available. This data set was also low-passed using a Lanczos-square filter with a 40-hour cutoff frequency to remove high-frequency components. The energy spectrum of low-passed sea level variations measured at Paranagua for the winter of 1984 (92 days) is presented in Figure 6. Subtidal sea level variations at that site appear to be strongly dominated by oscillations with a period of about 7 days, the same frequency band as the frontal systems, thereby giving support to the hypothesis that the frontal systems are in fact, one of the main low-frequency forcing mechanisms of the wintertime flow variability in the SBB.

3. A Conceptual Model of Cold Fronts for the SBB

The following mean characteristics of wintertime cold fronts in the SBB emerge from the analyses of the synoptic charts, of satellite imagery and coastal wind data: (1) the cold fronts which penetrate the southern part of

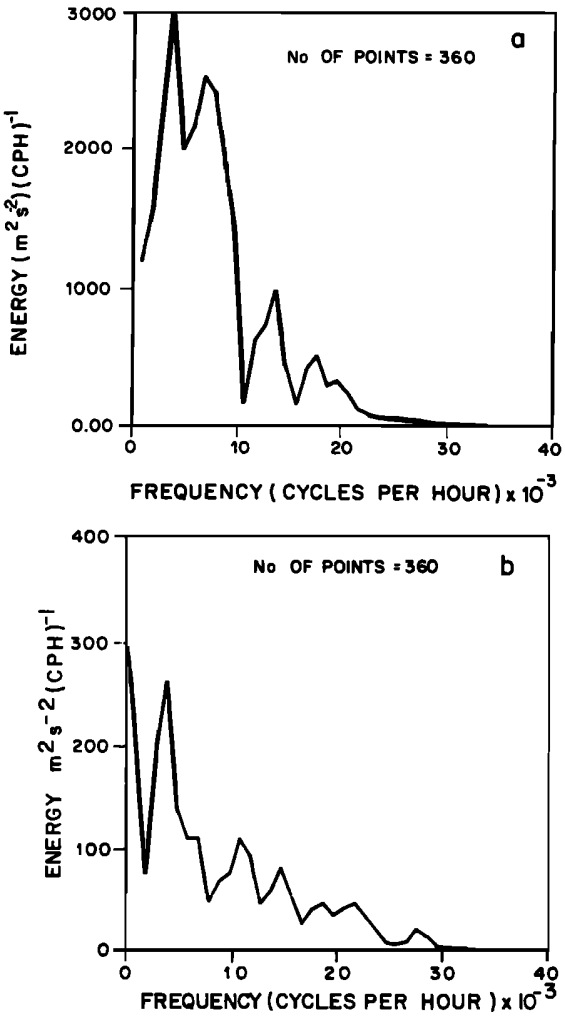

Fig. 3. Spectral energy density of the 40 Hour Low Pass (a) alongshelf and (b) cross-shelf wind components for the winter of 1984 at Santa Marta.

Brazil propagate from southwest to northeast in the alongshore direction of the SBB; (2) a mean 2-day travel time to cross the SBB gives these systems an average speed of 500 km d^{-1}; (3) in the warm sector of the front, the mean wind speed is 5 m s^{-1}, rotating counterclockwise from its dominant northeast direction to northwest with the approaching of the front; and (4) immediately after the passage of the cold front, the wind blows from southwest in the cold sector with a mean speed of 8 m s^{-1}, rotating counterclockwise from southwest to northeast approximately 1 day after the passage of the front.

This information has been synthesized into a conceptual model of wintertime cold fronts for the SBB. The conceptual model is a time and space dependent vector field, containing the basic characteristics of the wind field associated with the frontal passages. A schematic representation of such a model described above is shown in Figure 7. In the numerical experiments described subsequently, the finite element model is forced by this vector field.

4. The Numerical Model

The model used in this investigation was formulated by Wang and Connor [1975] and is a one-layer barotropic, two-dimensional f - plane model which uses the finite element technique to solve the dynamical equations of motion. The formulation is based on the Navier-Stokes equations for the conservation of momentum and a continuity equation for the conservation of mass of a fluid in rotation. The coordinate system is Cartesian, has its origin at the ocean surface with the x, y, and z axes pointing to east, north and vertically upward, respectively. The bottom topography is a function of the x and y coordinates. The fluid system consists of one layer of constant density. The vertical acceleration is neglected in the vertical equation of momentum by the hydrostatic approximation.

The following system of equations is obtained by the vertical integration of the equations of momentum and continuity from the bottom to the free surface:

$$\frac{\partial Q_x}{\partial t} + \frac{\partial uQ_x}{\partial x} + \frac{\partial vQ_y}{\partial y} = -gH\frac{\partial \eta}{\partial x} + \frac{1}{\rho}(\tau_{wx} + \tau_{bx}) + fQ_y + F_x$$

$$\frac{\partial Q_y}{\partial t} + \frac{\partial uQ_y}{\partial x} + \frac{\partial vQ_y}{\partial y} = -gH\frac{\partial \eta}{\partial y} + \frac{1}{\rho}(\tau_{wy} + \tau_{by}) - fQ_x + F_y \qquad (1)$$

$$\frac{\partial \eta}{\partial t} + \frac{\partial Q_x}{\partial x} + \frac{\partial Q_y}{\partial y} = 0$$

where Q_x and Q_y represent the integrated transport per unit of width for the x and y directions; u and v are the mean water column velocity components, η is the free surface anomaly, is the water density, τ_{wx} and τ_{wy} are the wind stresses, τ_{bx} and τ_{by} are the bottom stresses, and F_x and F_y are the integrated internal stresses. The wind and bottom stresses are both parameterized using quadratic formulations of the following forms

$$\vec{\tau}_w = \rho_{air} C_w |\vec{U}_{10}| \vec{U}_{10} \qquad (2)$$

where $C_w = (1.1 + 0.053\ U_{10}) \times 10^{-3} \times U_{10}$ [Wang and Connor, 1975] and U_{10} (meter per second) is the wind speed 10 m above the surface;

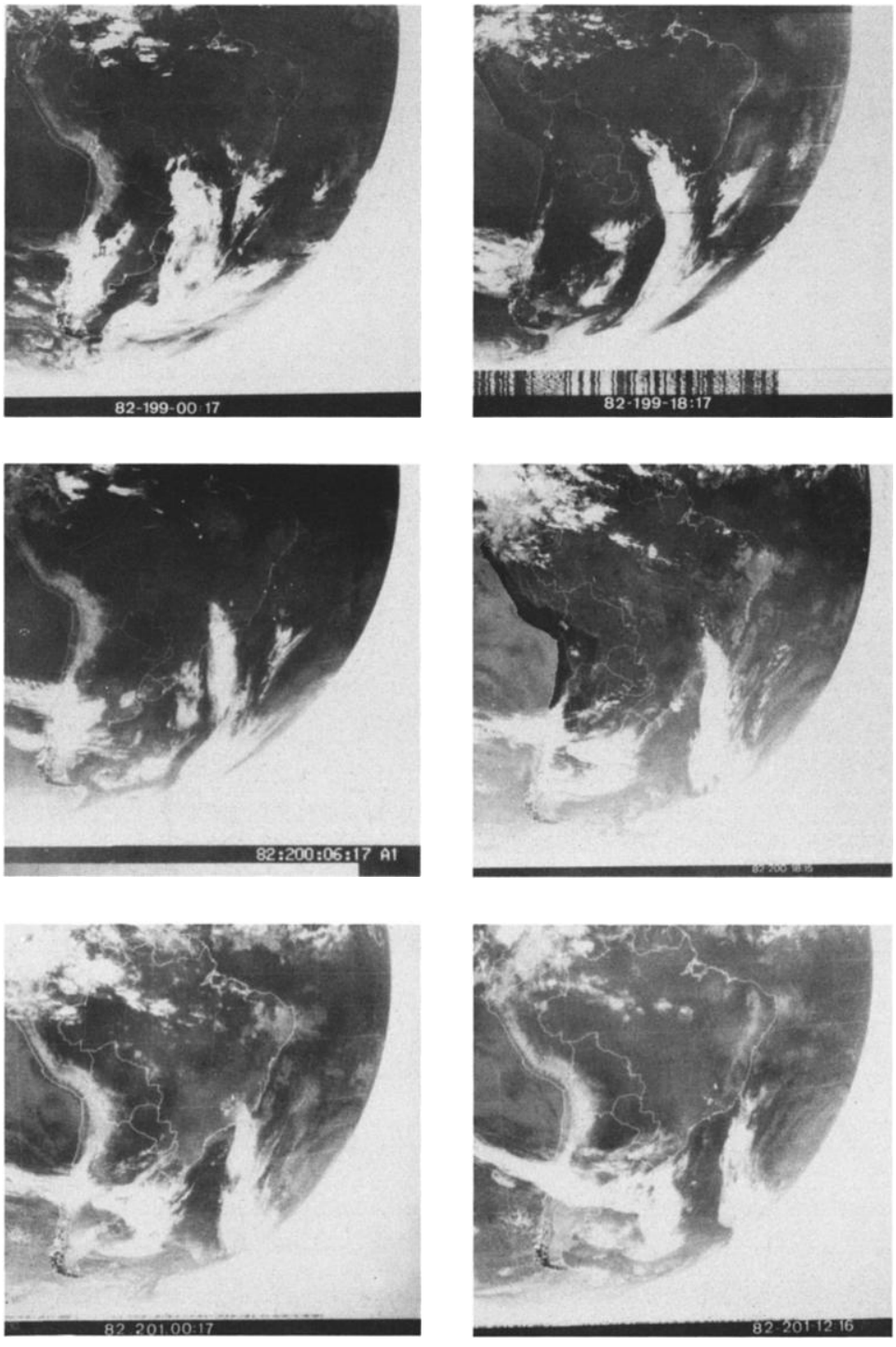

Fig. 4. A sequency of GOES-W IR imagery for the period from July 18, 1982, 0017 UT to July 20, 1982 1216 UT, showing a typical wintertime cold front propagation in southeastern Brazil.

$$\tau_{bx} = C_b(u^2 + v^2)^{1/2}\, u$$
$$\tau_{by} = C_b(u^2 + v^2)^{1/2}\, v \qquad (3)$$

where $C_b = 2.3 \times 10^{-3}$ [Hickey and Hamilton, 1980].

The following boundary conditions are used: (1) a radiation condition at the north and south boundaries normal to the coast [Orlanski, 1976], (2) an adiabatic condition of no sea surface elevation at the offshore boundary located at the shelf break [Beardsley and Haidvogel, 1981], and

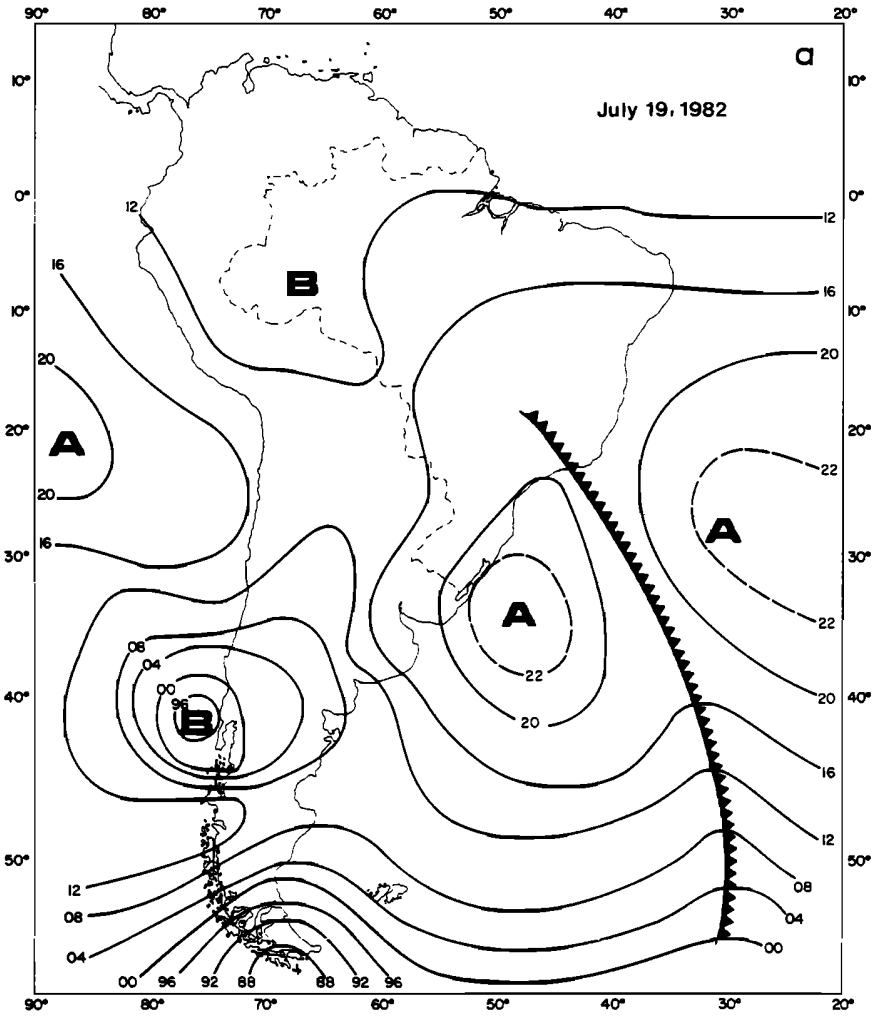

Fig. 5. Surface synoptic charts for (a) July 19, 1982, 1200 UT and (b) July 20, 1982, 1200 UT, for the southeastern Brazil. Low (high) pressure centers are indicated by B (A) in the figures. Units are hetoPascals, with the conventional meteorological use for values greater and smaller than 1000 hetoPascals.

(3) normal flow equal to zero at the coastal boundary.

5. Model Experiments

The region of interest was discretized using the grid of linear triangular elements shown in Figure 8; the bottom topography used in the model is presented in Figure 9. The 25°S latitude is used as the mean latitude in the model. The water density and horizontal eddy viscosity coefficients are set to $\rho = 1025$ kg m^{-3} and $A = 5 \times 10^2$ m^2 s^{-1}, respectively. The integration time step is $\Delta t = 300$ s. In order to minimize the effects of initialization, the model is forced for 36 h from rest, with a constant and uniform northeast wind of 5 m s^{-1}. A time ramp of 2 h is also used to bring the wind speed from zero to its 5 m s^{-1} value at the beginning of the integration. After the initial 36 h "warming up" of the model, the conceptual model of the cold front is then used to simulate the passage of a cold front which takes about 2 days time. After this, one and a half more days of a constant 5 m s^{-1} wind field are integrated, a situation corresponding to the return of normal undisturbed wind conditions.

5.1. Momentum Balance

With the wind stress forcing and the model generated current velocities and sea surface anomalies, the time series for each term of the momentum equations were obtained for analysis. In

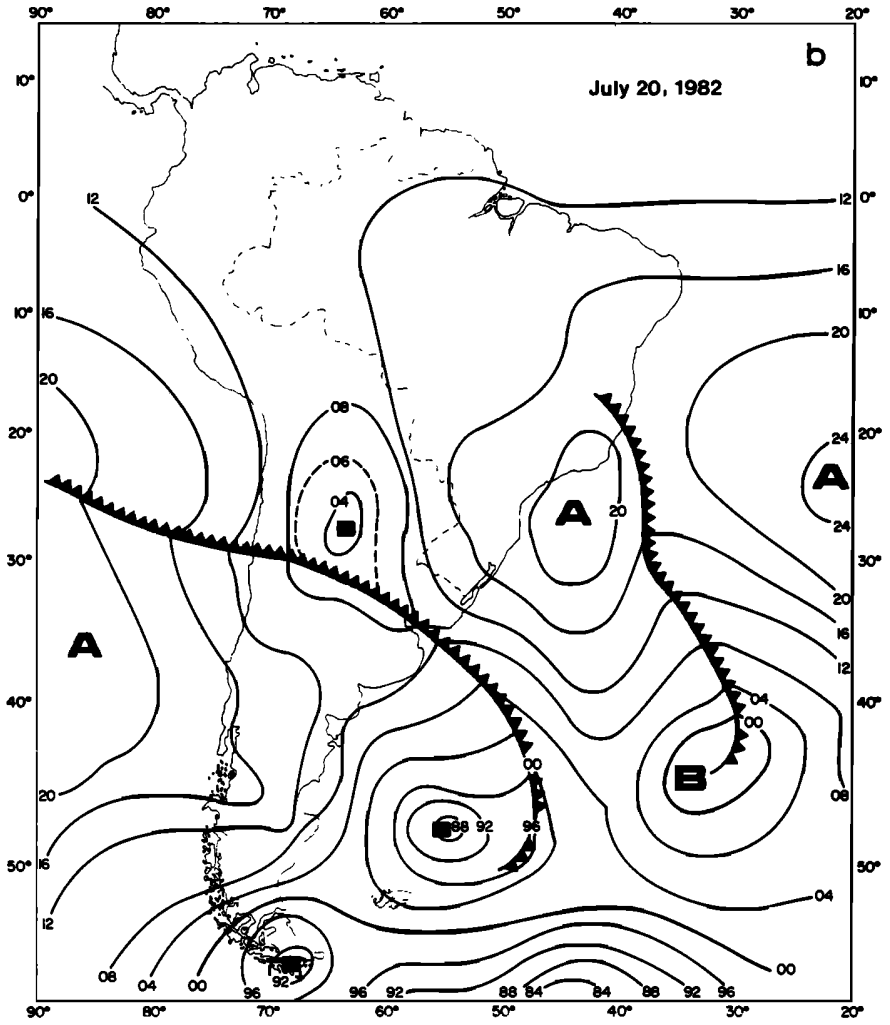

Fig. 5. (continued)

TABLE 1. Statistics of Wintertime Cold Fronts for the SBB

Year (Winter)	Number of Fronts	Mean Time Between Consecutive Fronts, Days	Time to Propagate Through the SBB, Days
1980	16	5.4	2.0
1981	11	6.9	2.1
1982	13	6.1	1.8
1983	13	6.2	1.9
1984*	8	6.3	1.9
1985	13	6.6	1.8

* Results are anomalous due to missing data for the month of August caused by problems in the satellite.

Figures 10, 11 and 12 these time series are plotted for the grid nodes 47, 63, and 65 (Figure 8) located at the 25-, 77- and 127-m isobaths, respectively.

The analysis of these time series for the first day and a half of integration, when the SBB was still under constant wind conditions, reveals that the steady state response of the region is characterized by a geostrophic balance for the cross-shelf direction throughout the region. For the alongshore direction, these plots indicate basically two distinct steady state dynamics: for the inner shelf where depth is small, the bottom friction increases and in the limit will tend to balance the alongshore wind stress; and for the mid and outer shelf, Ekman dynamics seems to

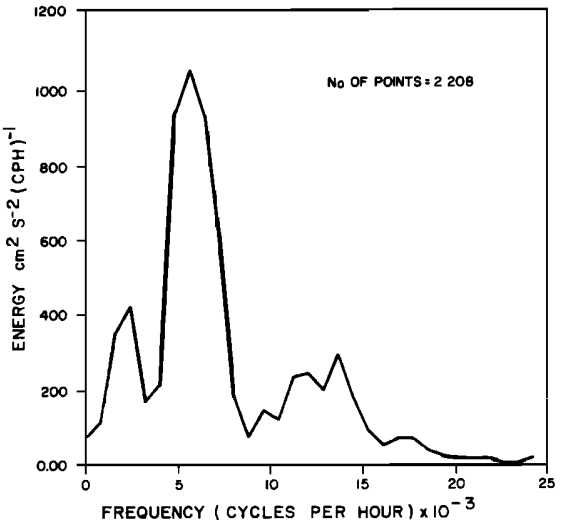

Fig. 6. Spectral energy density of the 40 Hour Low Pass sea level oscillations for the winter of 1984 at Paranagua.

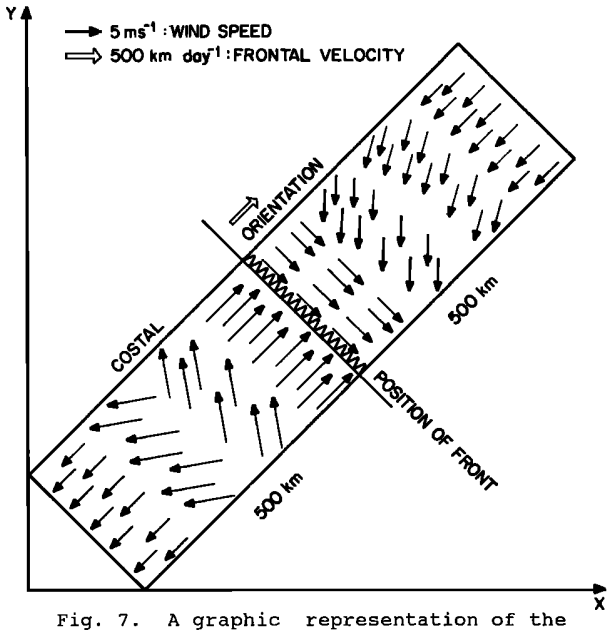

Fig. 7. A graphic representation of the conceptual model of wintertime cold front for southeast Brazil. The x and y axes point to east and north, respectively.

dominate the flow with the Coriolis term balancing the wind stress. An alongshore pressure gradient also seems to weakly contribute to this alongshore balance.

After one and a half days of integration, Figures 10, 11 and 12 reveal the strong influence of the frontal systems over the dynamics of the region. The frontal passage brings about a complete reversal in the flow and a local acceleration which is more concentrated in the alongshore direction for the inner and midshelf. It is interesting to note that for the cross-shelf direction, most of the geostrophic character of the flow is still preserved during the passage of the front with the pressure gradient and Coriolis fields changing together; the cross-shelf wind stress produced by the front tends to be balanced by a cross-shore acceleration of the flow.

Another interesting feature of these plots is the strong inertial oscillations (T = 28 hours) generated by the frontal passage. As expected, these oscillations increase in amplitude and become more circularly polarized with increased distance from the coast. The decaying time scale of these waves is directly proportional to the water depth, and seems to vary from 2 days for the outer shelf to 1 day for the inner shelf.

In order to obtain a representative estimate for the average value of each component in the momentum balance, each component has been averaged over the whole period of integration. The results obtained are presented in Tables 2 and 3.

Table 2 shows quite clearly the highly geostrophic character of the momentum balance in the cross-shelf direction. For the alongshelf direction, Table 3 shows that the wind stress, Coriolis force, pressure gradient force, local acceleration and bottom stress each should contribute to the momentum balance. While significant, the contribution of the bottom stress to the momentum equation is not clear-cut. The bottom stress, however, seems to be important for the inner shelf, where the depth is generally small; for nodes 126 and 150, the bottom stress is still important, despite the relatively large depths (H = 50 m and 117 m, respectively) since these nodes are located near the coast in the coastal jet.

5.2. Vorticity Balance

In order to obtain a better understanding of how the vorticity is being distributed and balanced in the system, the model results and the wind stress forcing were used to calculate the terms of the barotropic vorticity equation at each time step [Csanady, 1984]:

$$\frac{\partial \zeta}{\partial t} + u\frac{\partial \zeta}{\partial x} + v\frac{\partial \zeta}{\partial y} - f\frac{\partial \eta}{\partial t} = -g\left(\frac{\partial H}{\partial x}\frac{\partial \eta}{\partial y} - \frac{\partial H}{\partial y}\frac{\partial \eta}{\partial x}\right) + \left(\frac{\partial \tau_{wy}}{\partial x} - \frac{\partial \tau_{wx}}{\partial y}\right) - \left(\frac{\partial \tau_{by}}{\partial x} - \frac{\partial \tau_{bx}}{\partial y}\right) \qquad (4)$$

where $\zeta = \partial Q_y/\partial x - \partial Q_x/\partial y$.

Figure 13 shows the time series plots for each one of the terms of Equation (4) for different

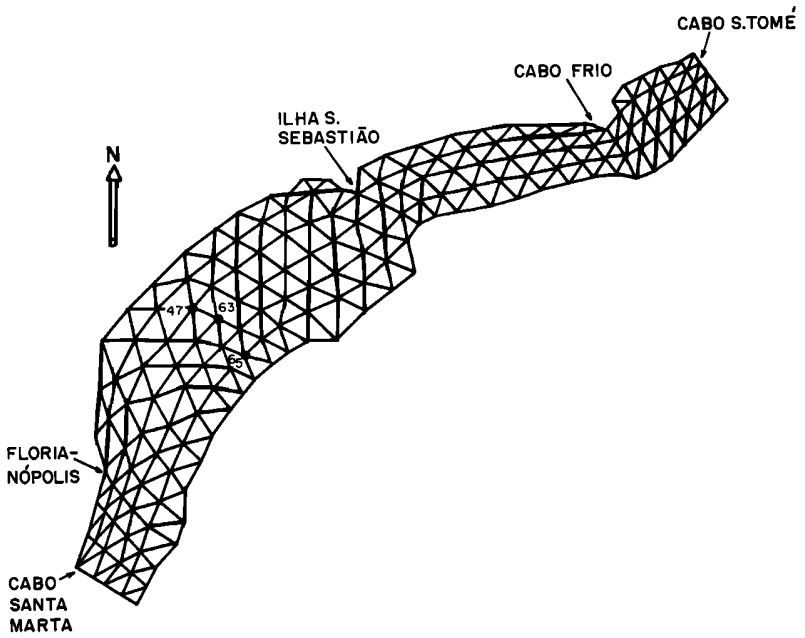

Fig. 8. Finite element grid for the South Brazil Bight. Number of nodes = 299 and number of elements = 188.

nodes. The most conspicuous feature in these plots is that vorticity is primarily generated by the topographic term (Jacobian), that is, by the stretching of the vortex filaments by the geostrophic flow crossing the isobaths. Even during the passage of the front, when the wind gains vorticity, a direct transfer of wind vorticity to the system seems to be only a secondary mechanism of vorticity generation for the flow. For the shallow region near the coast, these results indicate that the bottom frictional dissipation of vorticity is a very efficient mechanism for removing the vorticity generated by topographic stretching. Therefore for the inner shelf, a balance between the topographic vorticity generation and bottom frictional dissipation of vorticity dominates the flow. For the mid and outer shelf, with only a minor contribution from the bottom friction vorticity sink, the topographic vorticity is observed to generate a large local time rate of change of vorticity in the flow. The passage of the front introduces an oscillation in the vorticity field which has a time decay of a few days.

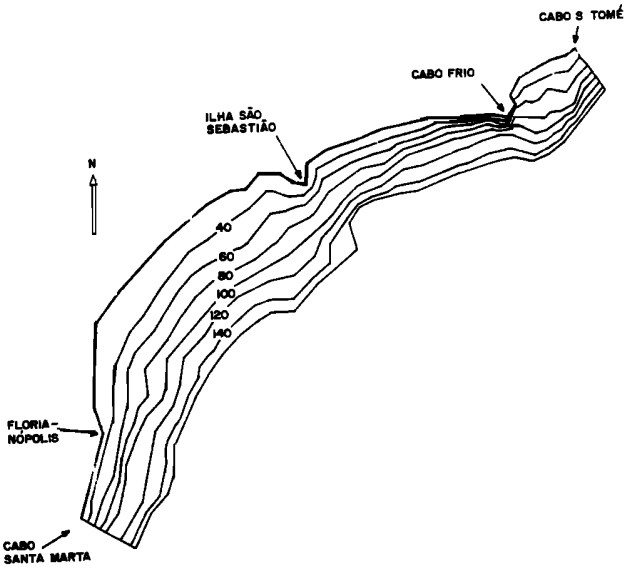

Fig. 9. Bottom topography used in the model. Contours in meters.

6. Discussion and Conclusions

The results obtained from the model indicate that the basic set of equations which describe the main mechanisms governing the wintertime dynamics of this region are

For momentum

$$fQ_y = gH \frac{\partial \eta}{\partial x} \tag{5}$$

$$\frac{\partial Q_y}{\partial t} + fQ_x = -gH \frac{\partial \eta}{\partial y} + \tau_{wy} - \tau_{by} \tag{6}$$

For vorticity

$$\frac{\partial \zeta}{\partial t} = -g\left(\frac{\partial H}{\partial x}\frac{\partial \eta}{\partial y} - \frac{\partial H}{\partial y}\frac{\partial \eta}{\partial x}\right) + \mathrm{curl}_k \vec{\tau}_w - \varepsilon \mathrm{curl}_k \vec{\tau}_b \tag{7}$$

where $\varepsilon = 1$ only in the inner and midshelf; otherwise $\varepsilon = 0$.

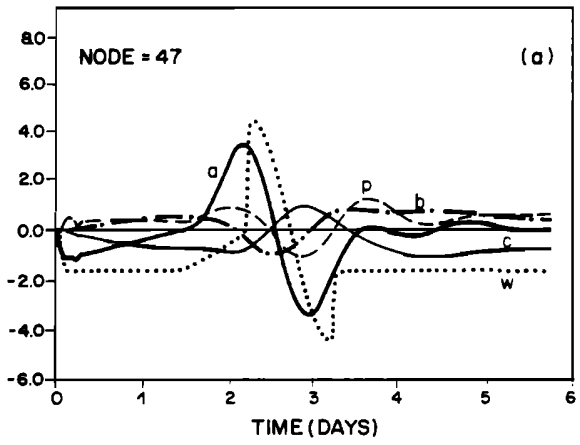

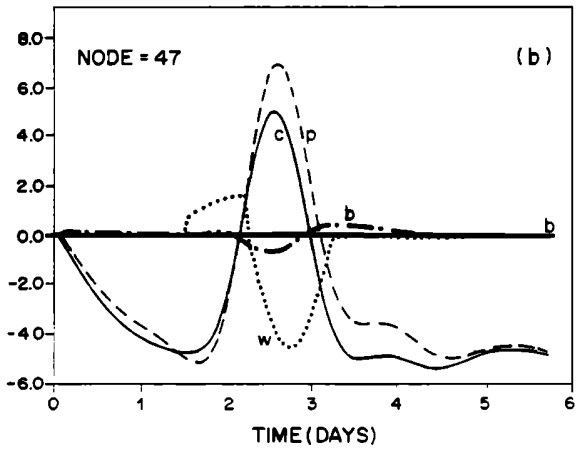

Fig. 10. (a) Alongshelf and (b) cross-shelf momentum balances at node 47 (Figure. 8) for the cold front experiment. Units are meters per second per second. Abbreviations are a = local acceleration term, c = Coriolis term (-fv and +fu for tne cross-shelf and alongshelf directions), p = pressure gradient term, w = wind stress term, b = bottom stress.

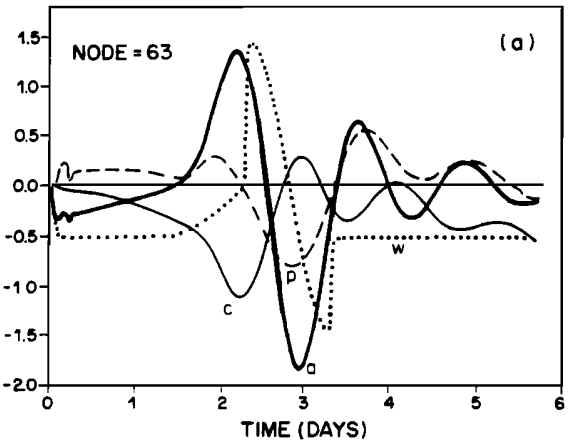

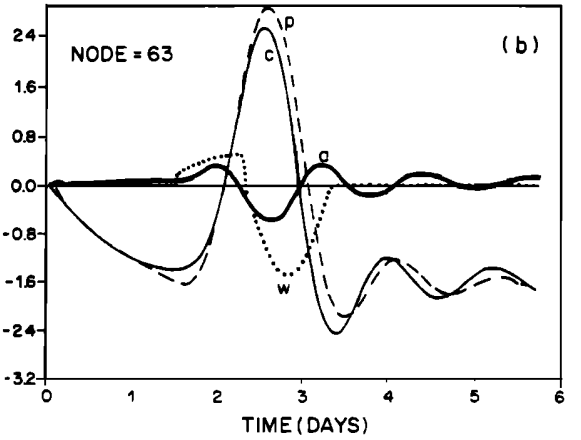

Fig. 11. As in Figure 10 except for node 63.

The results presented in section 5.1 show that the response of the SBB to the passage of wintertime cold fronts is quasi-geostrophic. For a barotropically dominated shelf, such as the SBB during the winter season, Klinck et al. [1981] show that its low frequency response to a moving system of wind stress is quasi-geostrophic if $\gamma = L_S/L_R < \pi^{-1}$, where $L_S = u_{system}/f$ and $L_R = (gh)^{1/2}/f$. For the case where $\gamma > \pi^{-1}$, the response is dominated by inertial waves.

Using typical values for the SBB, $L_S = 9.6 \times 10^4$ and $L_R = 5.2 \times 10^5$, one gets $L_S/L_R = 0.18$. This result indicates that the disturbances of the SBB produced by typical wintertime cold fronts should be quasi-geostrophic and that they should move with the storm. Both of these characteristics can be observed in the simulations. The inertial oscillations observed after the passage of the cold front in the simulations presented in this paper should not be confused with the inertial waves referred to by Klinck et al. [1981], which are supposed to be found during the passage of the front. Their model results are not valid for the decay of the currents after storm passage. A simple model is presented below to explain the origin of such observed inertial oscillations.

Equations (5) and (6), however, also indicate that the main momentum balance is very similar to that presented in most analytical models for wind-forced continental shelf waves [e.g., Gill and Schumann, 1974]. Therefore nonlocal effects produced by the propagation of long waves should not be neglected. In other words, a part of the subtidal changes in sea level and current variability at a specific point of this region cannot be explained only by the local winds.

Chao [1981] showed that energy leaks in the forward direction of shelf waves when the

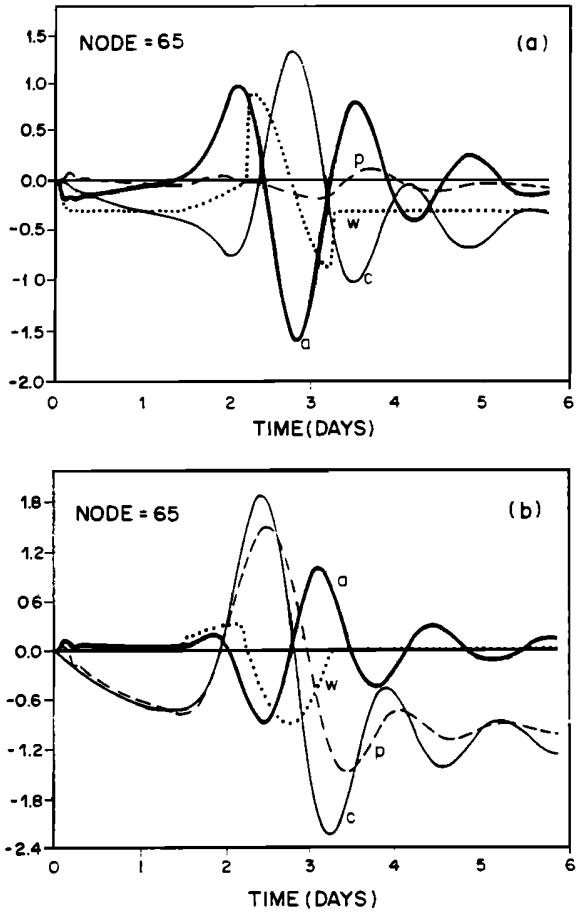

Fig. 12. As in Figure 10 except for node 65.

frequency of frontal passages is below the cutoff frequency of shelf waves. For the SBB, the frequency of frontal passages (2 /7 days) = 10^{-5} s^{-1} meets that condition, being well in the nondispersive region of shelf waves. Therefore the nonlocal effects should be expected. Castro Filho [1985] showed that for the SBB, the low-frequency coastal sea level fluctuations observed at one point are better correlated with the winds located to the south of it and at earlier times. These results also give some indication of the importance of remote forcing for the SBB.

For the inner and midshelf regions, the vorticity balance analysis shows that the main mechanism for vorticity generation is the topographic stretching term, with contributions from bottom friction dissipation of vorticity for the shallow nodes and local vorticity changes for the midshelf region. Analogous to the dynamics of shelf waves, wind vorticity does not seem important for these regions. For the outer shelf, where the Ekman dynamics seem to dominate the flow, wind vorticity is seen to be of importance, especially during the passage of cold fronts.

It is evident from Figures 10 to 12 (and others not presented herein) that a strong inertial signal is generated after the passage of the front. Also, the magnitude of this signal is strongly amplified with increasing water depth. Pollard and Millard [1970] show that the generation of inertial waves by winds can occur

TABLE 2. Time Mean of the Cross-Shelf Momentum Equation Terms

Terms Nodes (Depth)	Local Accel-eration	Advection	Coriolis	Pressure	Wind Stress	Bottom Stress	Eddy Viscos-ity
47(25)	0.33	0.22	-27.68	-21.12	-4.00	-0.58	-0.10
63(77)	0.12	0.05	-7.70	-6.70	-1.26	-0.05	-0.02
126(50)	-0.04	0.23	-42.00	-39.70	-1.57	-0.16	0.23
138(123)	-0.48	0.11	-17.58	-17.85	0.49	-0.02	0.03
150(117)	0.08	-0.13	-32.60	-33.04	1.48	-0.15	0.10
151(136)	0.52	0.60	-26.52	-26.15	0.70	-0.45	-0.45

Values are x 10^{-7} m s^{-2}.

TABLE 3. Time Mean of the Alongshelf Momentum Equation Terms

Terms Nodes (Depth)	Local Accel-eration	Advection	Coriolis	Pressure	Wind Stress	Bottom Stress	Eddy Viscos-ity
47(25)	-1.63	0.22	-5.37	1.16	-11.78	2.91	0.13
63(77)	-0.44	0.03	-2.57	0.55	-3.73	0.09	-0.10
126(50)	-3.18	0.06	-5.17	-7.31	-5.89	4.12	0.37
138(123)	-0.91	0.04	-0.85	-0.21	-2.10	0.42	0.11
150(117)	-1.67	0.05	-5.18	-5.69	-2.13	1.29	-0.41
151(136)	-1.47	0.24	-1.42	-1.63	-2.14	0.81	-0.01

Values are x 10^{-7} m s^{-2}.

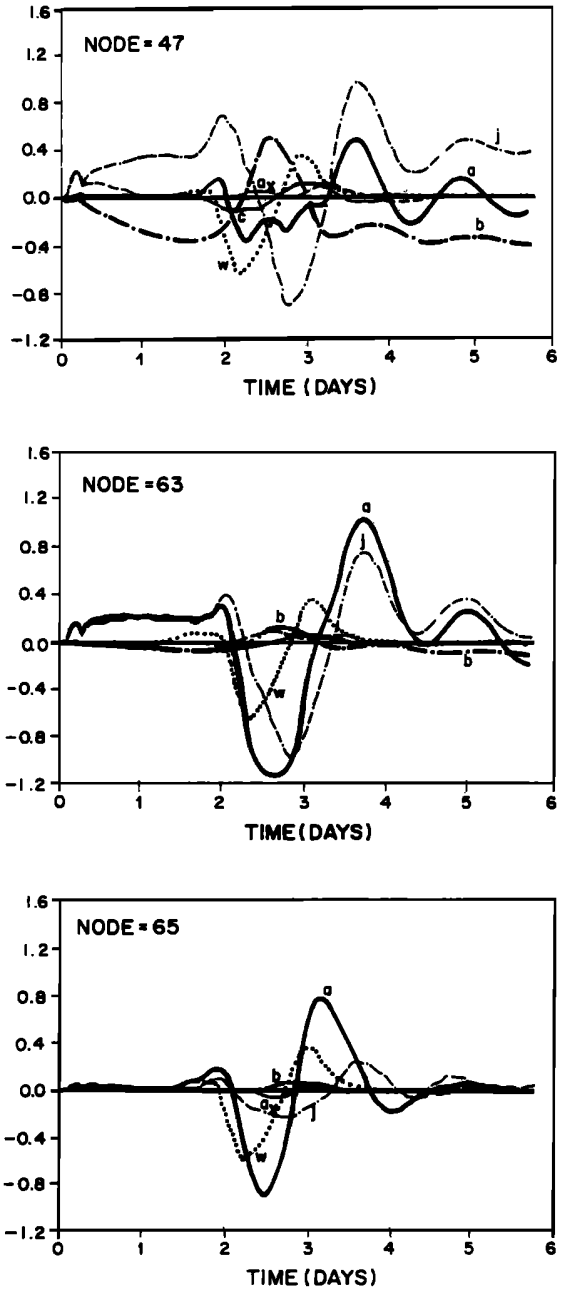

Fig. 13. Vorticity balance at nodes 47, 63 and 65 for the cold front experiment. Units are meters per second per second. Abbreviations are a = local rate of change, J = Jacobian, w = wind curl, b = bottom stress curl, a_x and a_y advectives terms.

in three different circumstances. First, an inertially rotating wind vector would generate an inertial current with continously increasing amplitude in a resonant situation. A second possibility is a strong wind blowing in one direction for a limited time, which could not be greater than half the inertial period. A third case would be a strong wind combined with a fairly sudden shift in direction. Theoretical models of inertial waves generated by impulsive winds are discussed, for example, by Gonella [1971] and Millot and Crépon [1981].

As may be inferred fro Figure 7, the passage of the frontal system introduces a rotation in the wind vector in the same direction of rotation expected for an inertial motion in the southern hemisphere (i.e., counterclockwise). Now Figure 7 shows that in the frontal system, the wind goes through a complete turn in 750 km. With a velocity of 500 km/d, this gives a period of T = 1.5 days for a complete wind rotation; or an angular frequency of $\omega = 2\pi/T = 0.49 \times 10^{-4}\ s^{-1}$, which is very near the inertial frequency of the system $f = -0.62 \times 10^{-4}\ s^{-1}$. It seems therefore a quite natural assumption to speculate about a resonance mechanism between the wind and the inertial mode of the system as one of the possibilities described by Pollard and Millard [1970].

In order to verify the resonance hypothesis, consider the vertically integrated, linearized momentum equations where the pressure gradient is neglected and the bottom friction is parameterized proportional to the water velocity. The following set of equations results:

$$\frac{\partial u}{\partial t} - fv = \left(\frac{\tau_{wx}}{\rho H}\right) - \left(\frac{ru}{\rho H}\right) \qquad (8)$$

$$\frac{\partial v}{\partial t} + fu = \left(\frac{\tau_{wy}}{\rho H}\right) - \left(\frac{rv}{\rho H}\right) \qquad (9)$$

Multiplying equation (9) by $i = (-1)^{1/2}$ and adding to equation (8) one gets

$$\frac{\partial V}{\partial t} + ifV + \left(\frac{r}{\rho H}\right)V = \frac{T(t)}{\rho H} \qquad (10)$$

where V is the vertical mean velocity of the water column (= u + iv), T the wind stress vector ($= \tau_x + i\tau_y$), r the bottom friction coefficient and H water depth.

Assuming that $T = Ae^{i\omega t}$ and that $V = V_o e^{i\omega t}$, the solution of equation (10) is

$$V(t) = \frac{(A/\rho H)}{[(\omega + f)^2 + (r/H)^2]^{1/2}} \exp[i(\omega t + B)] \qquad (11)$$

where

$$B = \frac{\pi}{2} - \tan^{-1}\left[-\frac{(r/H)}{(\omega + f)}\right] \qquad (12)$$

This solution shows that resonance can occur if $\omega + f \simeq 0$ and the bottom friction is small.

TABLE 4. Examples of Solutions for (11) Calculated Using Typical Values Generated by the Model

H, cm	v, cm/s	τ_b	r	|v(t)| f<0	|v(t)| f>0	|v(t)| f<0, ω=0	B
2500	10.0	2.3×10^{-1}	2.3×10^{-2}	12.6	1.8	3.2	55°
7700	5.0	5.8×10^{-2}	1.2×10^{-2}	5.0	0.6	1.1	81°
12500	3.5	2.8×10^{-2}	8.0×10^{-3}	3.0	0.4	0.7	87°

The $(\omega + f)$ term only will tend to zero for the southern hemisphere ($f < 0$) if $\omega > 0$, a situation of counterclockwise rotation of the wind, and $|\omega| \simeq |f|$. Using typical values of velocity and bottom stress taken from the momentum balance (Figures 10, 11 and 12) for nodes 47, 63, and 65, the following table shows the magnitude of the velocity (columns 5, 6 and 7) and phase (last column) as given by (11) and (12) for different conditions.

As observed in column 5 of Table 4, the velocity values given by the resonance theory compares well to the model results (column 2). For the same forcing in the northern hemisphere, column 6 shows very small velocity values. For stationary wind, column 7 gives the theoretical values for the southern hemisphere. Again, the psedicted values are substantially smaller than those given by the model. Therefore it seems quite possible that resonance might be in present, given the small difference between the wind frequency and the inertial mode.

It is interesting to note the reduction of the phase lag between the wind and the current, with the increase in bottom stress as the coast is approached (last column in Table 4). This solution indicates that near the coast, a balance between the wind and the bottom stress might dominate the flow with a current flowing in the direction of the wind with almost no phase lag. For the outer shelf, the solution indicates a phase lag of 90° typical of an Ekman balance. Both results agree with the previous analysis of the momentum balance.

For the narrower continental shelf region of the SBB to the north of São Sebastião, the momentum and vorticity balances are very similar to those presented for the wider region to the south. Inertial waves were also found to be present in model simulations for this northern sector. One important difference between these two domains is that in the northern part, probably due to its smaller cross-shelf dimension, the current field from the middle to the outer shelf regions is more intense than in the southern sector.

It should be noted that for the region extending from Cabo Frio to the northern boundary of the model domain, the conceptual cold front model may not sometimes represent adequately the wind characteristics of the region. For example, part of the cold fronts deviates offshore before reaching Cabo Frio. Some fronts that do reach Cabo Frio are already weakened, presenting only weak winds blowing from the southern quadrant. Therefore the results obtained for this region should be accepted with these restrictions in mind.

Finally, it should be said that some care must be exercised with regard to the results presented for the region near the shelf break, since in this region the Brazil Current plays an important role in the circulation, with an associated baroclinic field of mass, not accounted for in the model.

Acknowledgments. The authors wish to thank the Interministerial Commission for Marine Research (CIRM), Brazil, for its support of Project DINACO (9298) through which this paper was prepared; José Carlos Rodrigues for help in the development of the Cold Front Conceptual Model; Robert Beardsley of WHOI for a discussion which led to the proposition of the resonance mechanism of the inertial signals, and Merritt R. Stevenson, Yelisetty Viswanadham and Márcio L. Vianna, of INPE, for discussing and improving the manuscript, and Regina C. dos Santos for helping in typing and formatting this paper.

References

Beardsley, R. C. and D. B. Haidvogel, Model studies of wind-driven transient circulation in the Middle Atlantic Bight, 1, Adiabatic boundary condition, J. Phys. Oceanogr., 11, 355-375, 1981.

Castro Filho, B. M., Subtidal response to wind forcing in the South Brazil Bight during winter, Ph.D. thesis, 211 pp., Rosenstiel Sch. of Mar. and Atmo. Sci. Univ. of Miami, Miami, Fl., 1985.

Castro Filho, B. M., L. B. de Miranda, and S. Y. Miyao, Condições hidrográficas na plataforma continental ao largo de Ubatuba: variações

sazonais e em média escala, Bol. Inst. Oceanogr. Univ, São Paulo, 35(2), 135-151, 1987.

Chao, S. Y., Forced shelf circulation by an alongshore wind band, J. Phys. Oceanogr., 11, 1325-1333, 1981.

Clarke, A. J. and K. H. Brink, The response of stratified, frictional flow of shelf and slope waters to fluctuating large-scale, low-frequency wind forcing, J. Phys. Oceanogr., 15, 439-453, 1985.

Csanady, G. T., Circulation in the coastal ocean, 279 pp, D. Reidel Hingham, Mass., 1984.

de Miranda, L. B., Análise de massas de água da plataforma continental e da região oceÂnica adjacente: Cabo de São Tomé (RJ) a Ilha de São Sebastião (SP), Dissertação de Livre-Docência, 123 pp., Inst. Oceanogr. da Univ. de São Paulo, São Paulo, Brazil, 1982.

Garfield, N., III, The Brazil current at sub-tropical latitudes, Ph.D. thesis, 122 pp., Univ. of R. I., Narragansett, 1990.

Gill, A. E., and E. H. Shumann, The generation of long shelf waves by the wind, J. Phys. Oceanogr., 4, 83-90, 1974.

Gonella, J., A local study of inertial oscillations in the upper layers of the ocean, Deep Sea Res., 18, 775-788, 1971.

Hickey, B. M., and P. Hamilton, A spin-up model as a diagnostic tool for interpretation of current and density measurements on the continental shelf of the Pacific northwest, J. Phys. Oceanogr., 10, 12-24, 1980.

Ikeda, Y., and M. R. Stevenson, Seasonal characteristics of hydrography, turbulence and dispersion near Ilha Grande (RJ), Brazil, based on R/V Prof. W. Besnard data, Bol. Inst. Oceanogr. Univ, São Paulo, 31(1), 11-32, 1982.

Klinck, J. M., L. J. Pietrafesa, and G. S. Janowitz, Continental shelf circulation induced by a moving, localized wind stress, J. Phys. Oceanogr., 11, 836-848, 1981.

Leite, J. B. A., Estudos da variação temporal de temperatura e salinidade, do sistema de correntes e sua estabilidade numa área de ressurgência, Dissertação de Mestrado, 178 pp., Inst. Oceanogr. da Univ. de São Paulo, São Paulo, Brasil, 1983.

Matsuura, Y., Estudo comparativo das fases iniciais do ciclo de vida da sardinha-cascuda, Harengula Jaguana, (Pisces: Clupeidae) e nota sobre a dinamica da população da sardinha-verdadeira na região sudeste do Brasil, Dissertação de Livre-Docência, 150 pp., Inst. Oceanogr. da Univ. de São Paulo, São Paulo, Brazil, 1983.

Millot, C., and M. Crépon, Inertial oscillations on the continental shelf of the Gulf of Lions - Observations and theory, J. Phys. Oceanogr., 11, 639-657, 1981.

Orlanski, I., A simple boundary condition for unbounded hyperbolic flows, J. Comp. Phys., 21, 251-269, 1976.

Pollard, R. T., and R. C. Millard, Comparison between observed and simulated wind-generated inertial oscillations, Deep-Sea Res., 17, 813-821, 1970.

Stech, J. L., Um estudo comparativo da dinâmica da circulação de inverno entre as plataformas continentais das costas sudeste do Brasil e dos Estados Unidos utilizando um modelo numérico, Tese de Doutoramento, 227 pp., Inst. Oceanogr. da Univ. de São Paulo, São Paulo, Brazil, 1990.

Wang, J. D., and J. J. Connor, Mathematical modeling of near coastal circulation, Tech. Rep. 200, R. M. Parsons Lab., Mass.Inst. of Technol., Cambridge, 1975.

J. A. Lorenzzetti and J. L. Stech, Divisão de Ciências da Terra, Instituto Nacional de Pesquisas Espaciais, Secretaria Especial de Ciência e Tecnologia da Presidência da República, C. P. 515, São José dos Campos, 12201, SP, Brazil.

(Received June 11, 1991;
accepted August 18, 1991.)